Bioelectromagnetics 42:37–50 (2021)

Temperatures in Pigs During 3 T MRI Temperatures, Heart Rates, and Breathing Rates of Pigs During RF Power Deposition in a 3 T (128 MHz) Body Coil

Chie-Hee Cho [1,2]* Christian Grosse-Siestrup,[3] Jacek Nadobny,[4] Christian Lojewski,[5] Stefan Markus Niehues,[1] Matthias Taupitz,[1] Bernd Hamm,[1] and Peter Schlattmann[6]

[1]Department of Radiology, Charité—Universitätsmedizin Berlin, Berlin, Germany
[2]Institute for Diagnostic and Interventional Radiology, University Clinic Jena, Jena, Germany
[3]Institute for Occupational Medicine, Charité—Universitätsmedizin Berlin, Berlin, Germany
[4]Clinic for Radio-Oncology and Radiation Therapy—Hyperthermia, Charité—Universitätsmedizin Berlin, Berlin, Germany
[5]Department of Anesthesiology and Surgical Intensive Care Section, Klinik für Anästhesiologie mit Schwerpunkt operative Intensivmedizin, Charité-Universitätsmedizin, Berlin, Germany
[6]Institute for Medical Statistics, Programming and Data Science, University Clinic Jena, Jena, Germany

Exposure to radiofrequency (RF) power deposition during magnetic resonance imaging (MRI) induces elevated body-tissue temperatures and may cause changes in heart and breathing rates, disturbing thermoregulation. Eleven temperature sensors were placed in muscle tissue and one sensor in the rectum (measured in 10 cm depth) of 20 free-breathing anesthetized pigs to verify temperature curves during RF exposure. Tissue temperatures and heart and breathing rates were measured before, during, and after RF exposure. Pigs were placed into a 60-cm diameter whole-body resonator of a 3 T MRI system. Nineteen anesthetized pigs were divided into four RF exposure groups: sham (0 W/kg), low-exposure (2.7 W/kg, mean exposure time 56 min), moderate-exposure (4.8 W/kg, mean exposure time 31 min), and high-exposure (4.4 W/kg, mean exposure time 61 min). One pig was exposed to a whole-body specific absorption rate (wbSAR) of 11.4 W/kg (extreme-exposure). Hotspot temperatures, measured by sensor 2, increased by mean 5.0 ± 0.9°C, min 3.9; max 6.3 (low), 7.0 ± 2.3°C, min 4.6; max 9.9 (moderate), and 9.2 ± 4.4°C, min 6.1, max 17.9 (high) compared with 0.3 ± 0.3°C in the sham-exposure group (min 0.1, max 0.6). Four time-temperature curves were identified: sinusoidal, parabolic, plateau, and linear. These curve shapes did not correlate with RF intensity, rectal temperature, breathing rate, or heart rate. In all pigs, rectal temperatures increased (2.1 ± 0.9°C) during and even after RF exposure, while hotspot temperatures decreased after exposure. When rectal temperature increased by 1°C, hotspot temperature increased up to 42.8°C within 37 min (low-exposure) or up to 43.8°C within 24 min (high-exposure). Global wbSAR did not correlate with maximum hotspot. Bioelectromagnetics. 2021;42:37–50. © 2020 The Authors. Bioelectromagnetics published by Wiley Periodicals LLC on behalf of Bioelectromagnetics Society

Keywords: heart and breathing rate; pigs; radiofrequency power deposition; tissue temperature; thermoregulation

Conflicts of interest: None.

*Correspondence to: Chie-Hee Cho, Institute for Diagnostic and Interventional Radiology, University Clinic Jena, Am Klinikum 1, 07747 Jena, Germany. E-mail: chie-hee.cho@med.uni-jena.de

Received for review 4 January 2020; Accepted 11 November 2020

DOI:10.1002/bem.22311
Published online 20 December 2020 in Wiley Online Library (wileyonlinelibrary.com).

INTRODUCTION

In 2015, 118 magnetic resonance imaging (MRI) examinations per 1,000 inhabitants were performed in the United States [OECD, 2018], corresponding to a total of 37,780,000 examinations in a population of about 327

million [www.worldometers.info]. During MRI exposure to radiofrequency (RF) power signals at a specific absorption rate (SAR), body temperature can increase despite the use of dedicated software tools that intermittently switch off RF. At 3.0 T, or 128 MHz, patients have reported unpleasant heating sensations [Yamaguchi et al., 2019]. Superficial and deep 3rd degree burns have also been described [Franiel et al., 2006; Watari and Tokuda, 2018, US FDA Maude database (https://www.accessdata.fda.gov/scripts/cdrh/cfdocs/cfMAUDE/search.CFM)].

RF energy distributes nonuniformly in the body due to tissue heterogeneity and RF instrument properties [Shellock and Crues, 1987]. Energy absorption in MRI can be influenced by deep and heterogeneous tissue or sometimes lead to resonant-like energy absorption patterns [Gordon, 1984; National Council on Radiation Protection and Measurements, 1986; Michaelson and Lin, 1987; Gordon, 1988; Shuman et al., 1988].

The power density absorbed by tissue exposed to an RF field is expressed by the SAR, which is defined as the power absorbed per kilogram body mass (W/kg). Exposure thresholds have been defined as global or whole-body SAR (wbSAR) and local SARs for specific body regions.

RF superposition and reflection can lead to unequal distribution of SAR and local maxima in volumes known as hotspots [Shrivastava et al., 2011]. During RF exposure, multiple hotspots may occur in the human body [Nadobny et al. 2007]. Nadobny et al. [2015] reported about prediction of two hotspot areas (local SAR and temperature increases) in pigs: a dorsal hotspot (hotspot "1", see Table 1, last column) and a hotspot in the area of the right lateral ribs (hotspot "2", see Table 1, last column).

SAR limits are defined by the International Electrotechnical Commission (IEC) [2015] on the basis of model calculations and RF experiments with defined SARs in healthy human volunteers and animals, and aim at ensuring safe MRI examinations and avoiding thermal tissue damage [Lotz, 1985; Adair and Berglund, 1986; Kido et al.,1987; Shellock and Crues, 1987; Barber et al., 1990; Adair and Berglund, 1992; Shellock et al., 1994; van den Bergh et al., 2000; Adair et al., 2005; Shrivastava et al., 2008; Shrivastava et al., 2014; IEC, 2015]. The IEC 60601-2-33 [2015] standard defines three modes of clinical MRI examinations: a "normal operating mode" for all patients, a "first level controlled operating mode" applicable in patients with unimpaired thermoregulation who require supervision of the cardiovascular system, and a "second level operating mode" requiring ethics committee approval.

This standard allows a maximum body core temperature increase of up to 0.5°C with a maximum wbSAR of 2 W/kg in the "normal operating mode" and up to 1.0°C in the "first level controlled operating" mode with a maximum wbSAR of 4 W/kg and maximum local temperatures of 39°C in the trunk, 40°C in the extremities, and 38°C in the brain [IEC 60601-2-33, 2015].

Higher SAR levels than in the normal mode may be needed to achieve adequate image quality in abdominal MRI examinations. In such cases, the operator must decide whether the first level operating mode can be chosen based on the patient's thermoregulatory status. If this is not possible, imaging parameters can be modified to stay below the wbSAR threshold of the normal operating mode by changing the order of pulse sequence or increasing intervals between successive pulse sequences.

Although the whole-body SAR can be calculated directly from measurement of the transmitted RF power and coil efficiency, noninvasive determination of local SARs occurring during a routine clinical MRI examination is less precise and has a lower resolution compared with invasive measurement. Local SARs can be approximated by applying complex electromagnetic and biophysical calculations based on a realistic voxel model of the patient. Many computational models have been used to calculate the SAR in healthy human volunteers and animals [Adair and Berglund, 1986; Adair and Berglund,1992; Adair et al., 1998; Bernardi et al., 2003; Adair et al., 2005; Shrivastava et al., 2008; Shrivastava et al., 2014]. However, these models do not explicitly consider dynamic changes in heart and breathing rates. Thermoregulation may be delayed and is affected by a range of individual patient factors including sweating [Wang et al., 2007, 2008], training, fitness, and heart and breathing rates during the examination. None of the existing models can simulate individually different responses (including heart and breathing rates) to heat stress.

Therefore, we conducted a study focusing on the identification of individual ways of changes in tissue temperature, and heart and breathing rates during RF exposure by way of experimental validation using invasive intramuscular and rectal temperature measurement in 20 anesthetized pigs. These data may be the basis for developing more detailed bioheat models to better understand human thermoregulation and improve patient safety during MRI.

MATERIALS AND METHODS

Whole-Body RF Exposure System

A 16-ring bird-cage-type whole-body resonator of a conventional 3 T MRI system (MAGNETOM Trio; Siemens, Erlangen, Germany; 60 cm bore diameter,

operating frequency 123 MHz) driven in quadrature mode was connected to a 35 kW RF power amplifier via a 90° hybrid. RF was applied using a pulsed transmit scheme with a pulse peak power imitating a "sharp" RF pulse as used in routine MRI examinations (1 ms pulse duration). Defined SARs were accomplished by adjusting the duty cycle, i.e., the pulse repetition time (TR). Two directional couplers were inserted into the transmission line between the hybrid and the 0° and 90° resonator ports to monitor applied RF. Two pick-up coils, positioned opposite the input stage of the 0° and 90° resonator ports at the end ring of the bird cage, served to monitor coil efficiency. Further details of basic instrumentation can be found in Nadobny et al. [2015].

A network analyzer was used to determine the applied wbSAR. Prior to every experiment, a low-power wbSAR-Level had already been applied as a part of a standard MR-procedure to measure the load losses and to adjust the necessary forward power level to the required wbSAR level. Prior to every experiment, to determine the applied wbSAR, a network analyzer was used, measuring the load losses and adjusting the necessary forward power level to the required wbSAR level. This low-power wbSAR is reported in the experimental exposure levels; see Table 2. Net RF exposure duration (i.e., time during which power was switched on) was either 30 or 60 min. Total exposure durations, including short power interruptions, are provided in Table 2.

Swine as Animal Model

We used the pig as a model for the same reasons as Shrivastava et al. [2014]. Pigs have a metabolic rate of 52.2 W/m^2, which is similar to the human metabolic rate of 45 W/m^2; and, with an average surface area of 1.8 m^2, pigs have a total average metabolic rate of 81 W and a rectal temperature of 39°C [Mount, 1979]. The pig model is also suitable because of a rather similar body fat percentage (22.4 ± 3%) [Mitchell et al., 2000] compared with humans (24 ± 12%) [Wang et al., 2010]. It is postulated that swine, like humans, do not pant for thermoregulation [Mount, 1979].

Animals

The animal experiment (responsible: Grosse-Siestrup) was approved by the local committee on animal experimentation of the Berlin Office for Health and Social Affairs (LaGeSo). Twenty pigs, German Landrace (no. 7-26), with a mean mass of 70.5 ± 4.7 kg, comparable with the average male human mass, were chosen (Table 2). Each pig was allowed to acclimate for at least 7 days after arrival in the central animal facility of the Charité (certified by DQS, 313712 QM 15, Frankfurt a. M., Germany) to avoid anxiety, and was fasted for 12 h before induction of anesthesia.

All pigs were anesthetized with propofol (2%) and 0.05 mg/ml fentanyl, intubated for securing the airway, and allowed to breathe spontaneously without breathing assistance; for further details see Nadobny et al. [2015]. The depth of anesthesia was controlled by the corneal reflex response.

The pigs were positioned on their left side on the MRI scanner couch. Although the pigs were positioned inside the bore, there was no active cooling and no temperature increase.

Experimental Design

Before experiments were started, the personnel were trained on dead animals. Pigs were divided randomly into five groups (Table 2). Sham exposure group (SG), pigs no. 13, 14, and 15 received no exposure but were positioned in the bore resonator for 30 or 60 min (wbSAR of 0 W/kg). Low-exposure group (LG), pigs no. 17, 18, 19, 20, and 26 were exposed to a wbSAR just above the human thresholds for normal operating mode. Pigs no. 17–20 were exposed to a mean wbSAR of 2.7 W/kg for a mean of 56.3 min. Pig no. 26 was exposed to wbSAR of 2.6 W/kg for 36.4 min. Moderate-exposure group (MG), pigs no. 11, 12, 21, 22, and 25 were exposed to a wbSAR just above the human threshold for first-level controlled operating mode (mean wbSAR of 4.8 W/kg) for a mean of 31.2 min. High-exposure group (HG), pigs no. 8, 9, 10, 16, 23, and 24 were exposed to a wbSAR just above the human threshold for first-level controlled operating mode (mean wbSAR of 4.4 W/kg for a mean of 60.9 min). The net exposure time was 30 min in the MG and 60 min in the HG. Extreme-exposure, pig no. 7 was exposed to a wbSAR of 11.4 W/kg; exposure time was 18 min.

Measurements

Temperatures were measured in 2-s intervals starting before RF exposure and continuing until 20 min after exposure. Rectal temperatures were recorded with a Bowman-type thermistor probe (BSD Medical, Salt Lake City, UT); measurement accuracy ±0.2°C over a range of 25–52°C; 3-point calibration in a stirred water bath with a National Bureau of Standards-traceable standard temperature sensor (accurate to 0.05°C over a range of 0–60°C).

Hotspot temperatures were recorded with optical fiber sensors (Ø 0.5 mm, FOTEMP, Optocon, Dresden, Germany; measurement accuracy ±0.04°C (via individual calibration against NTC-based temperature probe) for a temperature range of 33–50°C). They were placed by Seldinger technique via 3-French catheters and

TABLE 1. Temperature Sensors, Sensors 2 and 11 are Used for the Present Experiment*

Temperature sensor no.	Position of sensors in the pig	Depth of sensor placement (cm)	Hotspot calculated[a]
1	Latissimus dorsi muscle, right side, cranial	3	1
2—hotspot (1)	Latissimus dorsi muscle, right side, center	3	1
3	Latissimus dorsi muscle, right side, caudal	3	1
4	Latissimus dorsi muscle, left side, cranial	3	1
5	Latissimus dorsi muscle, left side, center	3	1
6	Latissimus dorsi muscle, left side, caudal	3	1
7	Oblique abdominal muscle, right side, cranial	0.5	2
8—(2)	Oblique abdominal muscle, right side, center	0.5	2
9	Oblique abdominal muscle, right side, caudal	0.5	2
10	Oblique abdominal muscle, right side, caudal	0.5	2
11—(3)	Medial gluteal muscle, outside bore	10	
12—rectal	Rectal	5	

*Measurement carried out in cm depth. Numbering of the sensors in parentheses as used by Nadobny et al., [2015] (1st column).
[a]Hotspots calculated as reported by Nadobny et al. [2015].

inserted into the muscle at 3–4 cm depth as close as possible to the hotspot area; see Table 1.

The temperature sensors are listed in Table 1. The temperature measured by sensor 2 is called hotspot temperature. Only this sensor is evaluated because: (i) sensor 2 was positioned exactly in the central plane of the bore and birdcage resonator; (ii) all six sensors placed for hotspot "1" in the same pig exhibited similar time-temperature curves; only the maximal values were different, as seen in pig no. 16 (Fig. 1); (iii) sensors 6–10 were subcutaneously located, not representing core temperature, as they were positioned close to ribs, lungs, and skin; (iv) sensor 11 was located outside the birdcage shield. The temperatures measured by sensors 6–11 will be presented and discussed elsewhere.

Serum potassium, pH, and partial carbondioxide (pCO_2) were measured after placement of temperature sensors and prior to RF exposure, after RF exposure, and 20 min after the end of RF exposure by blood gas analysis (BGA) of venous blood (SG) and arterial blood (RF-exposed animals) (ABL 800 flex; Radiometer, Krefeld, Germany).

Statistical Analysis

A linear mixed model fit by restricted maximum likelihood (REML) with the distribution of hotspot temperatures or rectal temperatures as dependent variables was used [Brown and Prescott, 2006]. Covariates of interest were exposure level, exposure time, and combined exposure level and time. Calculations were performed with the "R" package Ime4 [Bates et al., 2015; R Core Team, 2017]. Descriptive analysis was performed using SPSS 25 (IBM, Armonk, New York, NY).

RESULTS

Rectal Temperatures

Rectal temperatures measured before, during, directly after exposure, and 20 min after exposure are compiled in Table 2. Unlike local hotspot temperature, rectal temperature continued to increase after exposure or during short breaks, except in the SG (Table 2). Rectal temperature curves (green curve in Fig. 2a–e, third column) showed a nearly linear increase during and even after RF exposure, which lasted for at least 20 min (Fig. 3). Rectal temperature increased only by 0.7 ± 0.2°C after 60 min in the normal mode (LG), 1.4 ± 0.4°C after 30 min in the first level operating mode (MG), and 1.4 ± 0.5 after 60 min in the first level operating mode (HG).

Hotspot Temperatures

Hotspot temperatures measured before, during, directly after exposure, and 20 min after exposure are compiled in Table 2. Unlike rectal temperatures, all hotspot temperatures decreased after exposure or during short breaks (Table 2). Maximum hotspot temperature increases were ΔT 6.3°C (LG, pig no 20), ΔT 9.9°C (MG, pig no. 21), and ΔT 17.9°C (HG, pig no. 23), (Fig. 3). Rectal temperature increases did not correlate with increases in hotspot temperatures; an increase of 1°C in the rectum was seen at mean: 37 min, hotspot temperature was mean 42.8°C, increase of 5.2°C (LG); 23 min, hotspot temperature was mean 44.9°C, increase of 6.8°C (MG); and 24 min, hotspot temperature was mean 43.8°C, increase of 6.0°C (HG). Nine of 16 RF-exposed swine (56%) showed hotspot temperatures above 42°C after 30 min (Table 2). Hotspot temperatures above 42.2°C occurred in all three exposure levels while

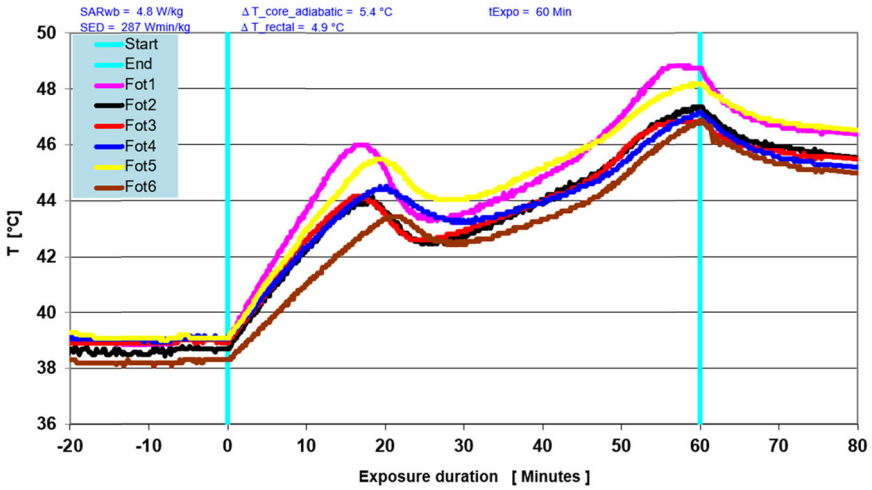

Fig. 1. Sensors 1–6 in a dorsal hotspot of pig no. 16 measure temperatures over time that result in a nonlinear, "sinusoidal," time-temperature curve.

rectal temperatures increased by a maximum of 1.78 ± 0.37°C. Hotspot temperatures cannot be predicted from the linearly increasing rectal temperatures. Mean hotspot temperatures of 42.6°C (LG, 60 min) and 45.0°C (MG, 30 min) already occurred when rectal (systemic) temperatures were still at "acceptable" levels of 40°C (LG) or 39.5°C (MG). At 18 min, hotspot temperature was 58.7°C (extreme-exposure pig). Pig no. 7 was not evaluated because planned RF exposure time (30 min) was not reached due to death after 18 min.

Heart Rate and Breathing Rate

Mean heart rate and breathing increased in LG, MG, and HG (Table 3). Pig no. 23 had a maximum breathing rate of 180 breaths per min (Table 4).

Time-Temperature Curve Shapes

Four distinct hotspot time-temperature curve shapes (sinusoidal, parabolic, plateau, and linear) were identified independent of the exposure group, and the curves were compared with breathing and heart rate responses for possible correlations. Furthermore, for systematic presentation, each of the four typical time-temperature curve shapes is represented by a simplified, "generic," curve in the left and middle columns with the corresponding exemplary actually-measured temperatures in the right column (Fig. 2).

The sinusoidal hotspot temperature curve occurred in the LG (pig no. 18), was not observed in the MG (30 min exposure time), and also occurred in the HG (pigs no. 8, 9, 10, 16). The sinusoidal curve (Fig. 2a) was the most commonly identified curve shape. It was associated with nonlinear increases in breathing rates (panting with more than 120 breaths/min, blue graph) and nonlinear increases in heart rates (red graph) during RF exposure. When RF was turned off, hotspot temperature slowly decreased linearly in all animals, the heart rate remained continuously high or even increased, and the breathing rate decreased slightly but continued to be high (Table 5).

The double sinusoidal hotspot temperature curve shape (Fig. 2e), seen in pig no. 24 (HG), was associated with nonlinear increases in breathing rates (panting with more than 120 breaths/min, blue graph) and no changes in heart rate (red graph) during RF exposure (Table 5). When RF was turned off, hotspot temperature slowly decreased linearly, heart rate remained constant, and breathing rate also remained constant (HG pig 24).

The parabolic hotspot temperature curve (Fig. 2b) occurred in the LG (pigs no. 17 and 19) and MG (pigs no. 22 and 25), and was not observed in the HG. Parabolic curves were observed during 30- and 60-min exposures. This curve shape was associated with nonlinear increases in breathing rates (panting with more than 120 breaths/min, blue graph) but with slight decreases in heart rate (red graph) during RF exposure. When RF was turned off, hotspot temperature slowly decreased linearly, heart rate stayed constantly high or even increased (like for sinusoidal curves), and breathing rate decreased slightly and then remained on a high level or was continuously high (Table 5).

The plateau-like hotspot temperature curve occurred in the LG (pigs no. 20 and 26) and MG (pigs no. 11 and 12), but was not observed in the HG. This curve shape (Fig. 2c) was also associated with nonlinear increases in breathing rates (more than 120 breaths/min, blue graph) but no changes in heart rate

TABLE 2. Hotspot and Rectal Temperatures Measured Before, at 30 min of RF Exposure, at End of RF Exposure, and 20 min After End of Exposure in the Different Exposure Groups

						Hotspot temperature (°C)				Rectal temperature (°C)			
Exposure group (n) mean	Pig numb-er*	Mass (kg)	wbSAR (W/kg	Exposure duration (min)	SAR (W* min/kg)	Before exposure	At 30 min of exposure	End of exposure	20 min after end of exposure	Before exposure	At 30 min of exposure	End of exposure	20 min after end of exposure
Sham ($n = 3$)	13(1)	73.0	0	30.0	0	39.4	39.6	39.5	39.7	38.9	39.0	39.0	39.0
	14(2)	67.0	0	60.0	0	37.8	37.8	37.9	37.8	37.7	37.3	37.2	37.0
	15(3)	68.8	0	60.0	0	38.7	39.1	39.3	39.4	38.0	38.0	38.2	38.3
Mean		69.6		50.0		38.6	38.8	38.9	39.0	38.2	38.1	38.1	38.1
Low ($n = 5$)	17(4)	61.0	3.1	65.0	194.0	37.8	42.6	43.1	41.5	38.3	39.0	40.6	40.9
	18(5)	70.2	2.5	60.0	154.0	38.3	41.8	42.2	41.2	38.5	39.1	40.3	40.7
	19(6)	67.5	2.6	60.0	156.0	38.0	42.9	42.4	40.8	38.3	38.8	39.9	40.3
	20(7)	65.5	2.6	60.0	155.0	36.3	41.4	42.6	39.8	37.3	38.1	39.2	39.2
	26(8)	78.0	2.6	36.4	94.8	37.6	42.9	42.7	40.3	38.5	39.4	39.8	39.9
Mean		68.4	2.7	56.3	150.8	37.6	42.3	42.6	40.7	38.2	38.9	40.0	40.2
Moderate ($n = 5$)	11	77.0	4.8	34.2	163.2	40.0	45.4	46.2	43.2	38.2	40.2	40.2	40.9
	12	73.7	4.9	31.2	156.0	39.1	45.9	47.8	45.0	39.1	40.0	40.4	41.5
	21(9)	70.5	4.8	30.5	144.0	36.6	46.5	46.5	44.5	36.9	37.9	37.9	38.3
	22(10)	62.5	5.2	30.0	156.0	38.0	43.4	43.4	40.7	38.4	39.9	39.9	40.4
	25(11)	73.0	4.2	30.0	127.0	36.7	41.0	41.3	39.3	38.0	39.2	39.1	39.8
Mean		71.3	4.8	31.2	156.7	38.1	44.4	45.0	42.5	38.1	39.4	39.5	40.2
High ($n = 6$)	8	70.0	4.6	61.7	285.0	37.9	42.4	45.0	43.3	38.2	40.3	41.8	41.3
	9	71.8	4.7	60.4	281.0	36.7	44.1	43.0	39.8	35.8	36.6	37.7	37.6
	10	71.0	4.5	65.0	282.0	37.1	42.1	46.2	44.1	37.9	39.7	41.8	42.2
	16(14)	75.5	4.8	60.0	287.0	38.7	42.8	47.4	45.5	39.1	40.6	43.0	43.9
	23(13)	78.0	3.7	60.1	228.0	38.0	48.0	55.9	50.7	38.7	39.7	40.9	40.6
	24(12)	68.0	4.0	60.0	248.0	38.3	45.6	44.4	43.5	38.3	39.2	40.8	41.6
Mean		71.4	4.4	60.9	257.9	37.8	44.2	47.0	44.5	38.0	39.4	41.0	41.2
Extreme ($n = 1$)	7	68.0	11.4	18.0	205.2	39.9		58.7	56.7	39.8	43.2 at time of death (18 min)		

RF = radiofrequency; SAR, specific absorption rate; wbSAR = whole-body specific absorption rate.

*Numbering of pigs in parentheses as used by Nadobny et al. [2015] (2nd column). Note that the total exposure time (5th row) is equal to either exactly 30 or 60 min where the power was switched on plus short interruptions with no-power (e.g., because of entering into the Faraday-cage room and checking if the infusion is working properly). Total absorbed whole body energy (6th row) is the total absorbed whole body energy in pig, including pre-measurements (before the actual exposure) using low-level SAR for estimation of the particular wbSAR value. It is obtained by summation of all consecutive wbSAR levels multiplied by corresponding time intervals.

(red graph) during RF exposure. When RF was turned off, hotspot temperature slowly decreased linearly, heart rate remained constant, and breathing rate decreased slightly in a nonlinear fashion and then stayed high or was continuously high (Table 5).

The linear hotspot temperature curve was not seen in the LG, but was observed in the MG (pig no. 21) and HG (pig no. 23). This curve shape (Fig. 2d) was also associated with constant breathing rates (no panting, blue graph) and no changes in heart rate (red graph) during RF exposure. When RF was turned off, hotspot temperature slowly decreased linearly, while heart rate and breathing rate remained constant (Table 5). Pig no. 21 showed a linear temperature increase of 10°C. Pig no. 23 showed a linear hotspot temperature increase, but with irregular heart rates and breathing rates.

Serum Potassium

Mean serum potassium was nearly unchanged in the SG with 4.0 ± 0.2 mmol/L. In the LG, potassium increased from 4.3 ± 0.3 mmol/L at the start of RF exposure to 4.7 ± 0.2 mmol/L 20 min after exposure. In the MG, potassium increased from 4.4 ± 0.4 mmol/L to 4.9 ± 0.5 mmol/L 20 min after RF exposure. In the HG, potassium increased from 4.2 ± 0.3 mmol/L to 5.5 ± 1.3 mmol/L (Table 6). The mean potassium

	A	B	C	Pig no.
a	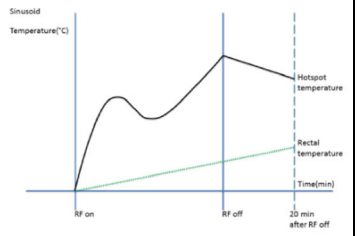	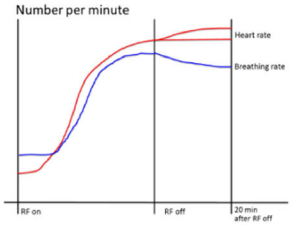	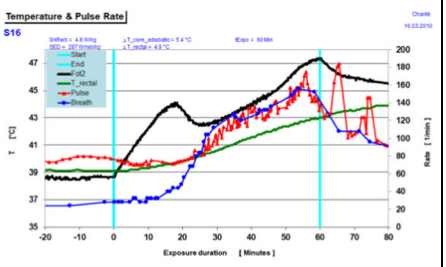	18-LG 8-HG 9-HG 10-HG 16-HG
b	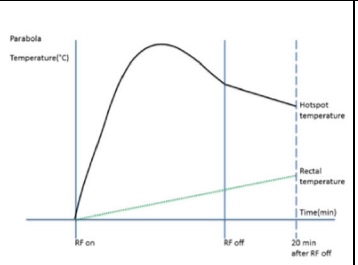	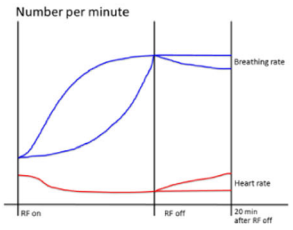	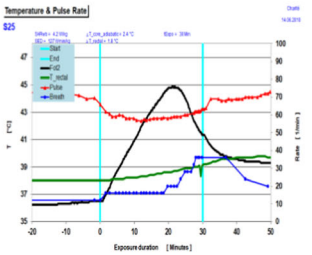	17-LG 19-LG 22-MG 25-MG
c	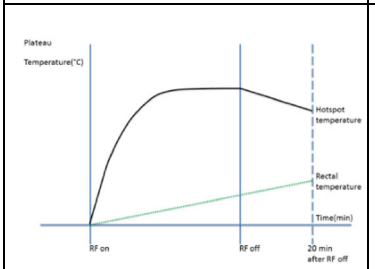	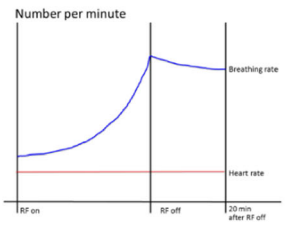	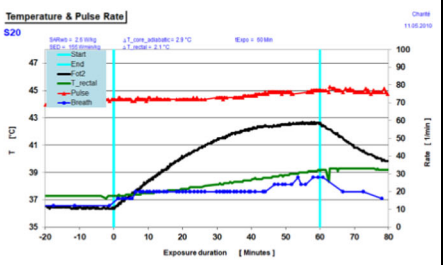	20-LG 26-LG 11-MG 12-MG
d	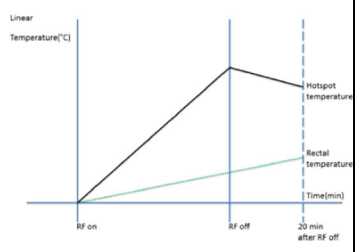	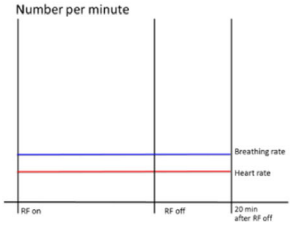	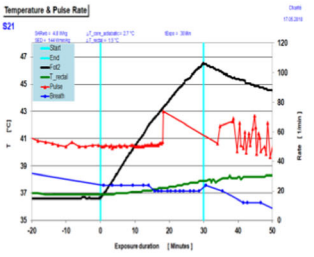	21-MF 23-HG
e	Double sinusoidal		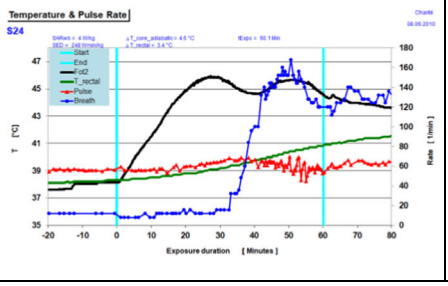	24-HG

Fig. 2. (**a**–**e**) Column A: schematic curve shape of hotspot (black) and rectal (green) temperature; B: schematic curve shape of breathing (blue) and heart (red) rates; C: exemplary real-time measurement in an exemplary pig (no. 16, 25, 20, 21, 24).

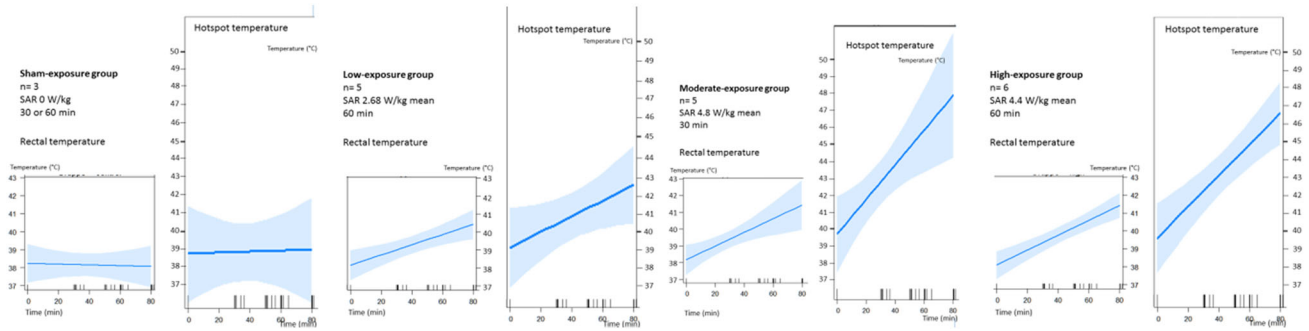

Fig. 3. Mean rectal and hotspot temperatures are represented by dark blue graphs and standard deviations (SDs) by light blue areas indicating SD width for each of the four exposure groups investigated.

increase was associated with increases in standard deviation (SD) (Fig. 4a).

pCO2 and pH

pCO2 decreased in the LG and HG, and increased in the MG (Table 6). pH stayed at 7.4 ± 0.0 from start to end of experiment, and until 20 min after end of exposure in the SG, MG, and HG. In the LG, pH increased from 7.3 ± 0.0 to 7.4 ± 0.0 (Table 6).

Statistical Analysis

Statistical analysis of the curve shapes (Fig. 3) precludes a linear correlation of temperatures with wbSAR. The REML method depicts the drift in rectal

TABLE 3. Heart and Breathing Rates of Pigs No. 7–26 Documented at the Start of Exposure, Maximum Heart and Breathing Rates During Exposure, at End of Exposure, and 20 min After Exposure*

		Heart rate				Breathing rate			
Exposure group (n) —mean	Pig number	Start of exposure	Maximum	End of exposure	20 min after end of exposure	Start of exposure	Maximum	End of exposure	20 min after end of exposure
Sham ($n = 3$)	13 (1)	83		77	89	20		24	28
	14 (2)	78		50	51	16		20	20
	15 (3)	61		60	64	36		36	40
Mean		74		62.3	68	24		27.7	29.3
Low ($n = 5$)	17 (4)	68	78	70	78	16	112	112	96
	18 (5)	77	190	90	96	20	64	48	64
	19 (6)	79		78	88	12		52	52
	20 (7)	72		77	75	16		28	16
	26 (8)	56		68	65	12		16	16
Mean		70.4		76.6	80.4	15.2		51.2	48.8
Moderate ($n = 5$)	11	55		57	76	16	60	48	
	12	62		55	74	24	136	112	108
	21 (9)	50		88	98	24		20	24
	22 (10)	79		88	78	16		32	M
	25 (11)	66		64	71	12		36	24
Mean		64.2		73.8	80.3	19		50	52
High ($n = 6$)	8	76		159	132	m	m	m	M
	9	52		73	81	m	m	m	M
	10	95		107	134	m		80	72
	16 (14)	75	162	139	92	28	156	152	96
	23 (13)	65	94	75	80	24	180	108	136
	24 (12)	60		53	64	8	168	96	132
Mean		70.5		110.6	103.8	20	168	109	109
Extreme ($n = 1$)	7	91				20			

*Missing value is m. Numbering of the pigs in parentheses as used by Nadobny et al. [2015] (2nd column).

TABLE 4. Hotspot and Rectal Temperatures in the Different Exposure Groups, Statistical Values for Figure 3

Hotspot temperatures			
Random effects: Number of observations: 76, Groups: no. of pigs 19			
Group		Variance	SD
Pig no.	(Intercept)	1.88	1.37
Residual		6.04	2.46
Fixed effects	Estimate	Std. error	*t* Value
(Intercept)	38.74	1.45	26.79
LG	0.39	1.83	0.21
MG	0.89	1.87	0.48
HG	0.82	1.77	0.46
Time	0.003	0.03	0.10
LG: time	0.04	0.03	1.21
MG: time	0.10	0.04	2.53
HG: time	0.09	0.03	2.78
Rectal temperatures			
Random effects: Number of observations: 76, Groups: no. of pigs 19			
Groups		Variance	SD
Pig no.	(Intercept)	1.18	1.09
Residual		0.16	0.39
Fixed effects	Estimate	Std. error	*t* Value
(Intercept)	38.24	0.66	58.12
LG	−0.09	0.83	−0.11
MG	−0.07	0.83	−0.09
HG	−0.16	0.81	−0.19
Time	−0.002	0.004	−0.52
LG: time	0.03	0.005	5.87
MG: time	0.04	0.01	6.69
HG: time	0.04	0.01	8.83

and hotspot temperature increases with increasing RF exposure levels from SG, LG, MG, to HG (Fig. 3). The SG has a linear, constant rectal and hotspot temperature; and temperatures measured in the rectum and hotspot temperatures increase with SAR. The mean increase is higher in the MG (SAR of 4.8 W/kg and 30 min) than in the HG (SAR, 4.4 W/kg and 60 min) (Fig. 4).

The graphs show the mean in dark blue with SD width in light blue. The SD width is attributable to the different time-temperature curves within the exposure groups. The SD of rectal temperatures was narrow compared to that of hotspot temperatures. The wide SD in the hotspot temperatures is due to the different composition of the time-temperature curves within the exposure groups, i.e., LG: two pigs sinusoidal, two pigs parabolic, and one pig plateau; MG: two pigs parabol, two pigs plateau, and one pig linear; HG: four pigs sinusoidal, one pig linear, and one pig double sinusoidal. In the SG, mean rectal and hotspot temperatures remained constant. REML of hotspot temperatures showed an increase with increasing RF intensity. With increasing RF intensity, rectal temperatures increased up to 43.9°C. SD width was greatest in the MG and smallest in the HG. As with hotspot temperatures, the REML showed narrower SD of rectal temperatures in the HG than in the LG or MG.

TABLE 5. Interaction of heart and breathing rates with thermoregulated hotspot curves

Curve	Heart rate	Breathing rate
Sinusoidal	Rises	Rises
Parabolic	Drops	Rises
Plateau	No change	Rises
Linear	No change	No change

DISCUSSION

LG, MG, and HG (pigs no. 7–12 and no.16–26) were exposed to RF energy with wbSAR levels slightly above the thresholds recommended by the IEC [2015]. The normal operating mode allows an exposure of 2 W/kg [IEC, 2015], which is comparable with the RF applied in LG (mean wbSAR of 2.7 W/kg over 60 min), and the first level controlled operating mode allows a wbSAR of up to 4 W/kg [IEC, 2015], which roughly corresponds to the experimental conditions in the MG and HG. The exposure time is the crucial difference between the MG (30 min) and HG (60 min). In clinical practice, the normal operating mode can be used in all patients undergoing an MRI examination, and the first level controlled operating mode is often chosen when a large volume such as the chest, abdomen, or spine is being imaged.

In some earlier studies, temperature changes in humans and animals were measured immediately before and after, but not during RF exposure [Lotz, 1985; Shellock and Crues, 1987; Adair et al., 2005; Shrivastava et al., 2008, 2011, 2014]. We measured temperatures before, during, and after RF exposure as did Shuman et al. [1988](dogs), Barber et al. [1990] (sheep), Shrivastava et al. [2014] (swine), as well as van den Bergh et al. [2000] and Shellock et al. [1994] (healthy human volunteers). Our investigation provides additional data on heart and breathing rates as well as blood electrolytes in order to identify patterns of response to bioheat stress.

Four Hotspot Time-Temperature Curve Shapes Were Identified: sinusoidal in five pigs (Fig. 2a), parabolic in four pigs (Fig. 2b), plateau in four pigs (Fig. 2c), and linear in two pigs (Fig. 2d). Time-temperature curve shapes were reported before, but not systematically classified: Adair and Adams [1980] and Adair et al. [2001] observed plateau-like temperature curve shapes for measurements performed at the body surface in humans. Another study found plateau curve shapes in the hotspot area of pigs [Shrivastava et al., 2014]. Under controlled

TABLE 6. Mean and Standard Deviation of Blood Gas Analysis; Sham Exposure Group Had Venous Blood Gas Analysis

	Exposure group	Start of exposure	End of exposure	20 min after end of exposure
Potassium	SG	4.0 ± 0.20	4.07 ± 0.11	4.17 ± 0.06
	LG	4.3 ± 0.27	4.7 ± 0.36	4.7 ± 0.17
	MG	4.4 ± 0.40	4.8 ± 0.34	4.9 ± 0.49
	HG	4.3 ± 0.34	5.0 ± 0.8	5.5 ± 1.3
pCO2	SG	60.9 ± 5.3	58.5 ± 9.3	56.4 ± 7.8
	LG	65.7 ± 8.3	57.8 ± 3.8	56.4 ± 7.3
	MG	50.1 ± 17.0	50.0 ± 2.1	54.2 ± 10.2
	HG	63.0 ± 3.9	50.1 ± 14.2	50.0 ± 7.9
pH	SG	7.4 ± 0.04	7.4 ± 0.05	7.4 ± 0.04
	LG	7.3 ± 0.03	7.4 ± 0.03	7.4 ± 0.05
	MG	7.4 ± 0.05	7.4 ± 0.03	7.4 ± 0.08
	HG	7.4 ± 0.04	7.4 ± 0.07	7.4 ± 0.04

breathing, temperature curves measured in dogs were nearly linear [Shuman et al, 1988]. Parabolic shapes were seen on the skin of sheep [Barber et al., 1990] and on the skin of the human hand in Shellock et al. [1994]. A linear increase in systemic (rectal) temperatures was also observed [Shuman et al., 1988; Barber et al., 1990] (Fig. 3). Sinusoidal curve shapes have not been reported by other investigators and may be due to the type of anesthesia we used (unassisted free breathing). The sinusoidal curve might indicate that the pigs were able to dissipate the heat from the hotspot, reducing the temperature for a restricted time, but then decompensated and hotspot temperature increased again. Only one animal (pig no. 24) had enough stamina to lower the increase for a second time but then also decompensated.

Hotspot Temperatures Above 42°C

Similar to Shuman et al. [1988] and Shrivastava et al. [2014], our measurements indicate that temperature in deeper tissues can be higher than subcutaneously. Both intramuscular hotspot and subcutaneous temperatures were reported to rise rapidly in sheep: Δ 6.0 ± 1.2°C (wbSAR, 4 W/kg at 1.5 T) [Barber et al., 1990]. They were similar to hotspot temperature changes of Δ 5.0 ± 0.9°C (LG, 60 min), Δ 6.4 ± 2.2°C (MG, 30 min), and Δ 9.2 ± 4.4°C (HG, 60 min) in our experiments. As we have seen a rapid rise in hotspot temperature, we agree with Barber et al. [1990] that there may be a need for different limits on RF intensities in different body areas.

Rectal Temperature Does Not Correlate With the Magnitude or Course of Hotspot Temperatures

We found a linear increase in rectal temperature ranging from 1.8 ± 0.4°C to 3.0 ± 0.9°C, which is higher than the linear rectal temperature increase in sheep of 0.025 ± 0.003°C/min for a wbSAR of 4 W/kg reported by Barber et al. [1990]. They observed the temperature increase (rectum and vena cava) to be proportional to wbSAR: and, according to their calculations, at 2 W/kg, "one hour would be needed to attain a 1°C rise in core temperature while about 30 min would be needed to achieve this increase at 4 W/kg." Shuman et al. [1988] also reported a linear rectal temperature increase.

We measured up to 39°C during a period of approximately 30 min, which is the time frame of a clinical MRI examination; however, during the same time interval, hotspot temperatures were already high: 40.5°C at 29 min in the LG, 41.6°C at 20 min in the MG, and 41.4°C at 21 min in the HG. Compared with the clinical situation, these observations in pigs suggest that temperatures exceeding 39°C can be reached before the end of a routine 30-min examination in the first level controlled operating mode.

Heart Rate and Breathing Rate Curves

Changes in heart and breathing rates are listed in Table 5. Mean resting heart rate of all pigs was 69 ± 12 beats/min and is comparable to the 70 beats/min reported by Mesangeau et al. [2000]. With increasing hotspot temperatures, 56% of the animals reacted with increasing heart rates. The heart rate increases with a sinusoidal curve (Fig. 2a) but drops in a parabolic curve (Fig. 2b); this may be due to an increase in the ejected blood fraction, which was not measured here.

In all animals, mean resting breathing rate before RF exposure was 18 ± 7 breaths/min, which is within the range reported by von Borell et al. [2007]. In pigs with parabolic curves, the breathing rate was increased while the heart rate was lower. The high breathing rates we measured in the pigs could be interpreted as panting. We observed that high breathing rates occur when the pigs are allowed to breathe freely as seen in all pigs with thermoregulation. We arbitrarily classify breathing rates above 50 breaths/min as panting. Two forms of panting

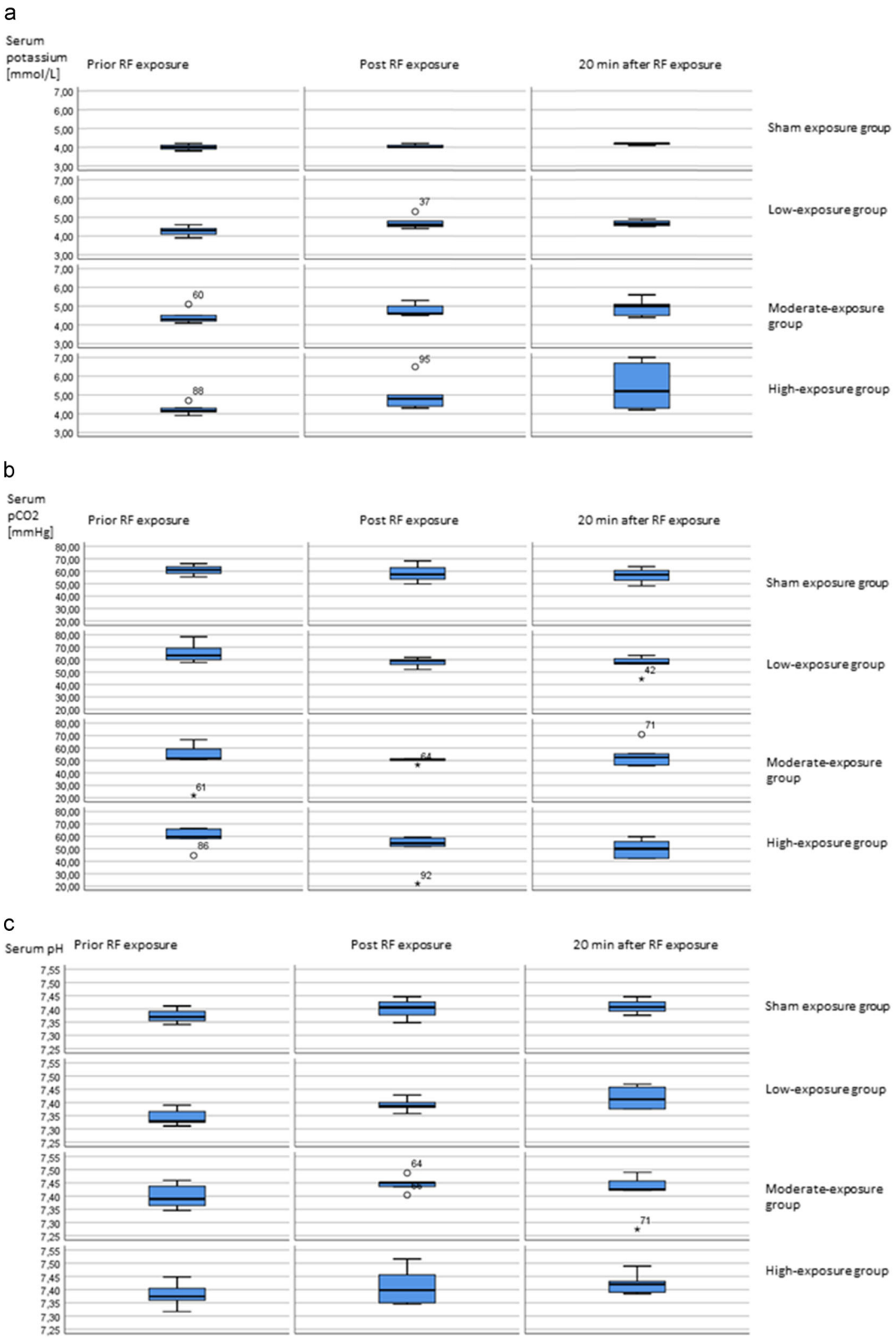

Fig. 4. (**a**) Changes in serum potassium levels prior, post, and 20 min after radiofrequency (RF) exposure. (**b**) Arterial mean pH levels prior, post, and 20 min after RF exposure. (**c**) Arterial partial carbondioxide (pCO_2) levels prior, post, and 20 min after RF exposure.

for thermoregulation, thermal tachypnea (first-phase panting, pCO_2 remains close to resting values, and up to 200–300 breaths/min may occur) and thermal hyperpnea (second-phase panting, pCO2 decreases), have been described by White [2018]. Pigs have been reported to wallow for thermoregulation [Mount, 1979]. No panting has been observed in pigs during RF exposure under assisted breathing anesthesia [Shrivastava et al., 2008, 2014].

Heart and breathing rates do not change in pigs showing linear increases in hotspot temperatures (Fig. 2d).

Serum Potassium, pCO_2, and pH

Setup and anesthesia do not influence serum potassium, pCO_2, or pH levels, as seen in the SG. Elevated temperatures induce an increase in breathing rates (in all groups) and lead to a decrease in pCO_2 and alkalosis (pH increases), most often seen in the HG (Fig. 4b), similar to thermal hyperpnea [White, 2018]. This results in the animal becoming alkalotic, and blood pH homeostasis becoming secondary to thermoregulation [White, 2018].

The pigs in the LG and MG had pH levels within close limits, while pigs in the HG had a wide range of pH responses immediately after RF exposure (Fig. 4c, last row). So what is the source of H^+? It comes from the exchange of serum potassium with intracellular H^+. Hotspot temperatures above 42°C cause cell damage, and intracellular potassium is depleted into the blood, as seen in the rise of serum potassium (Fig. 4a). Normally, high serum potassium leads to bradycardia, arrhythmia, and cardiac arrest (Table 3); instead, we observed tachycardia. To avoid high potassium levels and thus bradycardia, potassium is removed from the blood into intact cells [DuBose et al., 1995] in exchange for H^+, which in turn is released into the blood [Mahnensmith and Aronson, 1985]. This amount of H^+ is large enough to keep the pH within close limits (Table 6).

Limitations

The pig model is often used to ensure the greatest comparability with humans. However, there are limitations to this model. Pigs have more subcutaneous fat than human beings, resulting in higher insulation of deposited energy. They are bred for meat production and therefore have a lower capillary density than humans (118.48 vs. 459–1.468 capillaries/mm^2) [Kurnoth et al., 1994; McGuire and Secomb, 2003]. This may slow down heat dissipation from hotspots into pig muscle. Shrivastava et al. [2014] argue that different anatomical geometries (pig skull being two to five times thicker than human skull, and pig trunk being more cylindrical than the ellipsoid human trunk) may cause significantly different local RF exposure levels and tissue heating.

Another limitation could be the use of anesthesia; the SG pigs had a constant rectal temperature (Table 2). This observation may perhaps be attributable to the fact that pigs could breathe autonomously during our experiments, which was not the case in the study of Shrivastava et al. [2008]. It has been postulated that anesthesia affects thermoregulation by reducing the ability to lower body temperature (described for ketamine in monkeys) [Hunter et al., 1981]. On the other hand, a general influence of anesthesia on temperature behavior cannot be ruled out as the use of fentanyl and propofol induces a respiratory depression resulting in hypercapnia, which also explains the initial high pCO_2 (Fig. 4a) prior to RF exposure. It cannot be excluded that metabolic effects counteracted the anesthesia-induced decrease in temperature.

Another limitation is the difference between anesthetized (healthy) animals and nonanesthetized humans (patients) undergoing MRI examinations. Underlying diseases (e.g., cardiovascular diseases [Rowell, 1983], diabetes [Barany, 1955], obesity [Buskirk et al., 1965]), or medications [Jauchem, 1985] alter thermoregulation.

CONCLUSION

RF exposure at 4 W/kg in 20 anesthetized pigs leads to hotspot temperatures exceeding 40°C, which is above accepted IEC limits. The hotspot temperature courses show four different curve shapes (sinusoidal, parabolic, plateau, and linear), which are influenced by breathing and heart rates. Rectal temperatures are lower and delayed compared to hotspot temperatures. Possibly, patient safety may be improved by online body core measurement to guide MRI, and individually adapt SAR exposure (higher or lower) for each patient.

ACKNOWLEDGMENTS

The authors are deeply indebted to Gerhard Brinker (Siemens, Erlangen, Germany) for technical and logistic support. We thank Siemens for support, Rafael Poschmann for editing the figures, and Bettina Herwig for language polishing. Sarah Ribéreau, Friederike Kobelt, Markus Piaskowski, and Katja Reiter assisted in conducting the experiments. We are grateful to the authors of Nadobny et al. [2015] for their work; however, some formal aspects of their

publication did not conform with the rules of the Charité (conciliation committee).

REFERENCES

Adair ER, Adams BW. 1980. Microwaves modify thermoregulatory behavior in squirrel monkey. Bioelectromagnetics 1:448–461.

Adair ER, Berglund LG. 1986. On the thermoregulatory consequences of NMR imaging. Magn Reson Imaging 4:321–333.

Adair ER, Berglund LG. 1992. Predicted thermophysiological responses of humans to MRI fields. Ann NY Acad Sci 649:188–200.

Adair ER, Blick DW, Allen SJ, Mylacraine KS, Ziriax JM, Scholl DM. 2005. Thermophysiological responses of human volunteers to whole body RF exposure at 220 MHz. Bioelectromagnetics 26:448–461.

Adair ER, Kelleher SA, Mack GW, Morocco TS. 1998. Thermophysiological responses of human volunteers during controlled whole-body radio frequency exposure at 450 MHz. Bioelectromagnetics 19:232–245.

Adair ER, Mylacraine KS, Cobb BL. 2001. Human exposure to 2450 MHz CW energy at levels outside the IEEE C95.1 standard does not increase core temperature. Bioelectromagnetics 6:429–439.

Barany FR. 1955. Abnormal vascular reactions in diabetes mellitus; a clinical physiological study. Acta Med Scand Suppl 304:1–129.

Barber BJ, Schaefer DJ, Gordon CJ, Zawieja DC, Hecker J. 1990. Thermal effects of MR imaging: worst-case studies on sheep. Am J Roentgenol 155:1105–1110.

Bates D, Maechler M, Bolker B, Walker Sl. 2015. Fitting linear mixed-effects models using lme4. J Stat Softw 67:1–48.

Bernardi P, Cavagnaro M, Pisa S, Piuzzi E. 2003. Specific absorption rate and temperature elevation in a subject exposed in the far-field of radio-frequency sources operating in the 10-900-MHz range. IEEE Trans Biomed Eng 50:295–304.

Brown H, Prescott R. 2006. *Applied Mixed Models in Medicine*, Second Edition. Chichester, UK: John Wiley & Sons. pp 1–430.Wiley.

Buskirk ER, Lundegren H, Magnusson L. 1965. Heat acclimatization patterns in obese and lean individuals. Ann N Y Acad Sci 131:637–653.

DuBose TD, Codina J, Burges A, Pressley TA. 1995. Regulation of H(+)-K(+)-ATPase expression in kidney. Am J Physiol 269:F500–F507.

Franiel T, Schmidt S, Klingebiel R. 2006. First-degree burns on MRI due to nonferrous tattoos. AJR Am J Roentgenol 187:W556.

Gordon CJ. 1984. Thermal physiology. In: Biological Effects of Radiofrequency Radiation. Washington, DC: EPA-600/8-83-026A. p4-1-4-28.

Gordon CJ. 1988. Effect of radiofrequency radiation exposure on thermoregulation. In: Joe A. Elder, Daniel F. Calill, editors. ISI Atlas Sci Plants Anim 1:245–250. Health Effects Research Laboratory Office of Research & Development. https://books.google.de/books/about/Biological_Effects_of_Radiofrequency_Rad.html?id=TKIKAQAAMAAJ&redir_esc=y

Hunter WS, Holmes KR, Elizondo RS. 1981. Thermal balance in ketamine-anesthetized rhesus monkey *Macaca mulatta*. Am J Physiol 241:R301–R306.

International Electrotechnical Commission (IEC). 2015. Medical electrical equipment—Part 2-33: -Particular requirements for the basic safety and essential performance of magnetic resonance equipment for medical diagnosis. International Electrotechnical Commission 60601-2-33-ed3.0b (3rd ED3.0b).

Jauchem JR. 1985. Effects of drugs on thermal responses to microwaves. Gen Pharmacol 16:307–310.

Kido DK, Morris TW, Erickson JL. 1987. Physiologic changes during high field strength MR imaging. Am J Roentgenol 148:1215–1218.

Kurnoth T, Salomon FV, Gille U. 1994. [Quantitative changes in the capillary supply of selected muscles of turkeys, ducks, rats and swine during postnatal development]. Anat Histol Embryol 23:21–39.

Lotz WG. 1985. Hyperthermia in radiofrequency-exposed rhesus monkeys: A comparison of frequency and orientation effects. Radiat Res 102:59–70.

Mahnensmith RL, Aronson PS. 1985. The plasma membrane sodium-hydrogen exchanger and its role in physiological and pathophysiological processes. Circ Res 56:773–788.

McGuire BJ, Secomb TW. 2003. Estimation of capillary density in human skeletal muscle based on maximal oxygen consumption rates. Am J Physiol Heart Circ Physiol 285:H2382–H2391.

Mesangeau D, Laude D, Elghozi JL. 2000. Early detection of cardiovascular autonomic neuropathy in diabetic pigs using blood pressure and heart rate variability. Cardiovasc Res 45:889–899.

Michaelson SM, Lin JC. 1987. *Biological Effects and Health Implications of Radiofrequency Radiation*. New York, NY: Plenum Press. pp 523–537.

Mitchell AD, Scholz AM, Pursel VG. 2000. Dual-energy X-ray absorptiometry measurements of the body composition of pigs of 90-130-kilograms body weight. Ann N Y Acad Sci 904:85–93.

Mount LE. 1979. *Adaptation to Thermal Environment. Man and His Productive Animals*. London: Edward Arnold (Publishers). pp. 146, 182–208.

Nadobny J, Klopfleisch R, Brinker G, Stoltenburg-Didinger G. 2015. Experimental investigation and histopathological identification of acute thermal damage in skeletal porcine muscle in relation to whole-body SAR, maximum temperature, and CEM43 °C due to RF irradiation in an MR body coil of birdcage type at 123 MHz. Int J Hyperthermia 31:409–420.

Nadobny J, Szimtenings M, Diehl D, Stetter E, Brinker G, Wust P. 2007. Evaluation of MR-induced hot spots for different temporal SAR modes using a time-dependent finite difference method with explicit temperature gradient treatment. IEEE Trans Biomed Eng 54:1837–1850.

National Council on Radiation Protection and Measurements. 1986. Biological effects and exposure criteria for radiofrequency electromagnetic fields. Report 86. Bethesda, MD: National Council on Radiation Protection and Measurements.

OECD. 2018. Magnetic resonance imaging (MRI) exams. Available from https://data.oecd.org/healthcare/magnetic-resonance-imaging-mri-exams.htm. [Last accessed 1 April 2018].

R Core Team. 2017. R: A language and environment for statistical computing. R Foundation for Statistical Computing, Vienna, Austria. Available from https://www.R-project.org/. [Last accessed 1 April 2018].

Rowell LB. 1983. Cardiovascular aspects of human thermoregulation. Circ Res 52:367–379.

Shellock FG, Crues JV. 1987. Temperature, heart rate, and blood pressure changes associated with clinical MR imaging at 1.5 T. Radiology 163:259–262.

Shellock FG, Schaefer DJ, Kanal E. 1994. Physiologic responses to an MR imaging procedure performed at a specific absorption rate of 6.0 W/kg. Radiology 192:865–868.

Shrivastava D, Hanson T, Kulesa J, Tian J, Adriany G, Vaughan JT. 2011. Radiofrequency heating in porcine models with a "large" 32 cm internal diameter, 7 T (296 MHz) head coil. Magn Reson Med 66:255–263.

Shrivastava D, Hanson T, Schlentz R, Gallaghar W, Snyder C, Delabarre L, Prakash S, Iaizzo P, Vaughan JT. 2008. Radiofrequency heating at 9.4T: In vivo temperature measurement results in swine. Magn Reson Med 59:73–78.

Shrivastava D, Utecht L, Tian J, Hughes J, Vaughan JT. 2014. In vivo radiofrequency heating in swine in a 3T (123.2-MHz) birdcage whole body coil. Magn Reson Med 72:1141–1150.

Shuman WP, Haynor DR, Guy AW, Wesbey GE, Schaefer DJ, Moss AA. 1988. Superficial- and deep-tissue temperature increases in anesthetized dogs during exposure to high specific absorption rates in a 1.5-T MR imager. Radiology 167:551–554.

van den Bergh AJ, van den Boogert HJ, Heerschap A. 2000. Skin temperature increase during local exposure to high-power RF levels in humans. Magn Reson Med 43:488–490.

von Borell E, Langbein J, Després G, Hansen S, Leterrier C, Marchant-Forde J, Marchant-Forde R, Minero M, Mohr E, Prunier A, Valance D, Veissier I. 2007. Heart rate variability as a measure of autonomic regulation of cardiac activity for assessing stress and welfare in farm animals—A review. Physiol Behav 92:293–316.

Wang Z, Heymsfield SB, Chen Z, Zhu S, Pierson RN. 2010. Estimation of percentage body fat by dual-energy X-ray absorptiometry: Evaluation by in vivo human elemental composition. Phys Med Biol 55:2619–2635.

Wang Z, Lin JC, Mao W, Liu W, Smith MB, Collins CM. 2007. SAR and temperature: Simulations and comparison to regulatory limits for MRI. J Magn Reson Imaging 26:437–441.

Wang Z, Lin JC, Vaughan JT, Collins CM. 2008. Consideration of physiological response in numerical models of temperature during MRI of the human head. J Magn Reson Imaging 28:1303–1308.

Watari T, Tokuda Y. 2018. MRI thermal burn injury: an unrecognized consequence of wearing novel, high-tech undergarments. QJM 1:495–496.

White MD. 2018. Panting as a human heat loss thermoeffector. Handb Clin Neurol 156:233–247.

www.worldometers.info. Population of United States. Available from http://www.worldometers.info/world-population/us-population/. [Last accessed 1 April 2018].

Yamaguchi T, Abe Y, Ichino Y, Satoh S, Masuda T, Kimura S, Ito M, Yamamoto T. 2019. Heating sensation in patients with and without spinal fixation devices during MRI examination at different magnetic field strengths. J Magn Reson Imaging 49:525–533.